Energy & Environmental Science

Accepted Manuscript

This article can be cited before page numbers have been issued, to do this please use: M. Norouzi Banis, H. yadegari, Q. Sun, T. Regier, T. Boyko, J. Zhou, Y. Yiu, R. Li, Y. Hu, T. Sham and X. Sun, *Energy Environ. Sci.*, 2018, DOI: 10.1039/C8EE00721G.

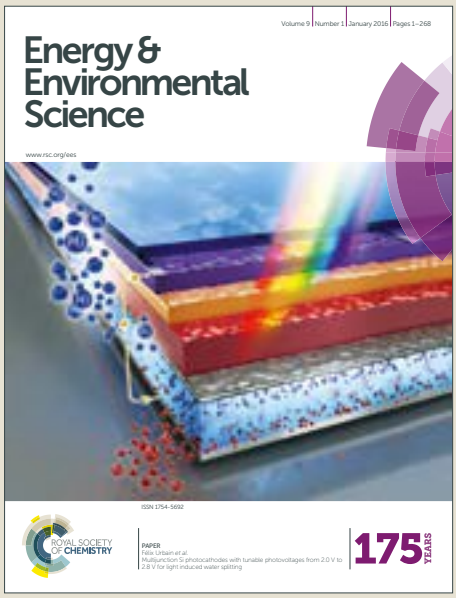

ROYAL SOCIETY OF CHEMISTRY

rsc.li/ees

View Article Online
DOI: 10.1039/C8EE00721G

Journal Name

ARTICLE

Revealing the charge/discharge mechanism of Na-O2 cells by in situ soft X-ray absorption spectroscopy

Received 00th January 20xx,
Accepted 00th January 20xx

DOI: 10.1039/x0xx00000x

www.rsc.org/

Mohammad N. Banis[†ac], Hossein Yadegari[†a], Qian Sun[a], Tom Regier[d], Teak Boyko[d], Jigang Zhou[d], Yun M. Yiu[b], Ruying Li[a], Yongfeng Hu[d], Tsun K. Sham[bc], Xueliang Sun*[a]

Developing high energy density batteries, such as metal-air systems, requires a good understanding of their underlying electrochemical principles. In-situ characterization methods provide valuable insight toward discharge/charge mechanism of Na-O_2 cells. However, previous application of soft X-ray absorption spectroscopy has been limited to ex-situ studies on the discharge products of the cell. Here we report an in-situ soft X-ray absorption technique for Na-O_2 cells to study the formation and decomposition of the discharge products during battery cycling. Taking advantage of the elemental selectivity and chemical sensitivity of soft X-ray absorption spectroscopy, we reveal the instability of discharge products in the Na-O_2 cell environment. Our results illustrate that in-situ soft X-ray absorption spectroscopy is an efficient probe to study the electrochemical mechanism of alkali metal-O_2 energy storage systems.

Introduction

The search for new energy storage systems has intensified the research on sodium-oxygen (Na-O_2) batteries.[1-5] The electrochemical mechanism of Na-O_2 cells as well as the physicochemical parameters affecting the performance of this system have been extensively studied.[6-15] During the discharge process of a Na-O_2 cell, dissolved oxygen reduces in the positive electrode and combines with Na^+ to produce solid sodium oxide(s) as the discharge product through electrochemical reactions. Subsequently, the discharge product decomposes to original Na^+ and O_2 upon charging.[2, 12] Although the general mechanism of Na-O_2 has been established, some aspects of the cell chemistry remains ambiguous[6, 9, 12, 15]. Unlike Li-O_2 batteries where Li_2O_2 has been widely accepted as the major discharge product in non-aqueous electrolytes, various compounds have been reported for Na-O_2 system, including sodium superoxide (NaO_2)[2, 7, 10, 13, 16], sodium peroxide (Na_2O_2)[2, 16, 17], hydrated form of peroxides ($Na_2O_2.2H_2O$)[18], sodium carbonate (Na_2CO_3)[17, 19] and mostly hybrid forms of these compounds.[17, 19, 20] The diversity of discharge products in Na-O_2 cells mainly originates from the relative instability of NaO_2 in the cell environment. However, the mechanism behind the degradation process of the discharge products is not clear. Meanwhile, ex-situ analysis of the highly sensitive discharge products is generally affected by contaminations from surrounding environment. Accordingly, effective in-situ characterization techniques are required to provide an accurate understanding of the decomposition mechanisms involved in Na-O_2 cells

Soft X-ray absorption spectroscopy (XAS) provides appropriate selectivity and sensitivity required for analytical tracing of the products in Na-O_2 cells[16]. XAS reveals information about the local electronic and chemical structure of products by probing states near the Fermi level using X-rays.[12, 16] In the present work, we developed an in-situ system for soft XAS study of non-aqueous Na-O_2 cells to examine the degradation mechanism of discharge products. The ultra-high vacuum condition employed in this technique eliminates any potential source of contamination, providing accurate and reliable chemical information on the electrochemical mechanism of the cells. Using in-situ soft XAS (mapping) measurements in conjunction with electrochemical characterization and ex-situ electron microscopy, we show that a progressive degradation reaction occurs at the products/electrolyte interface.

Results and discussion

The Na-O_2 cell employed in this study was built using the high vacuum compatible liquid cell developed by Canadian Light Source (CLS), to collect O and Na K-edge XAS (Fig.1a) on the high resolution spherical grating monochromator (SGM) beamline at CLS[21]. In-situ Na-O_2 cell was fabricated using Na metal as the negative electrode and an Au coated (30nm) silicon nitride window (100nm) as the positive electrode in a diglyme-based electrolyte.

[a] Department of Mechanical and Materials Engineering, Western University, London, Ontario, Canada.
[b] Department of Chemistry, Western University, London, Ontario, Canada.
[c] Soochow-Western Centre for Synchrotron Radiation Research, Western University, London Ontario, Canada.
[d] Canadian Light Source, Saskatoon, Saskatchewan, Canada.
† These authors contributed equally to this work.
* Corresponding Author, email: xsun9@uwo.ca
Electronic Supplementary Information (ESI) available: [Experimental and supporting information figures]. See DOI: 10.1039/x0xx00000x

View Article Online
DOI: 10.1039/C8EE00721G

Two most common discharge products in Na-O_2 cells are NaO_2 and Na_2O_2, where Na cations combine with superoxide (O_2^-) and peroxide (O_2^{2-}) anions respectively. The difference in the electronic configuration of the anions (Fig. 1b) is the unpaired electron in π^* of the O_2^- ions[22]. O K-edge XAS arises from excitation of O 1s electrons to unoccupied states of O 2p character (such as π^* and σ^* antibonding states)[12, 16]. Superoxide exhibits a peak at relatively low energies (~532eV) corresponding to transition to the partially filled π^* states and a broad peak at higher energies (~536eV) attributed to transition to the σ^* states[12, 23]. However, peroxide exhibits no π^* transition due to its completely filled π^* states.

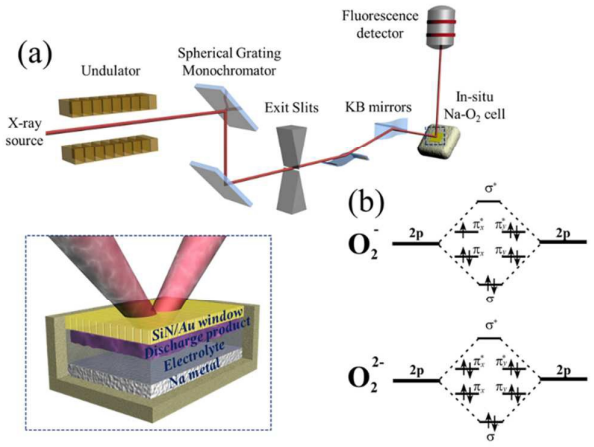

Figure 1. (a) schematic diagram of the Na-O_2 liquid cell designed for in-situ soft XAS studies, (b) electronic configuration of superoxide (top) and peroxide (bottom) anions.

Initially, O K-edge XAS spectra of other components of the cell, including electrolyte and solid sodium salt were recorded to track any potential interferences with XAS spectra of discharge products in the cell. (Fig. S1, Supporting Information). There is no overlap between these features and the characteristic features attributable to the Na-O_2 cell discharge products.

The possibility of damage and other effect induced by X-ray beam on the performance of Na-O_2 cell was tracked by monitoring the open circuit voltage (OCV) of the cell at various beam energies (Fig. S2, Supporting Information). The results indicate minimal changes in the OCV of the cell during XAS measurement, implying a consistent electrochemical reaction mechanism. The measurement time of each scan was limited to 30 seconds to minimize the beam damage on the discharge products and cell electrolyte.

Figure 2 shows the in-situ XAS results for Na-O_2 cell during discharge and charge cycles. All spectra show a broad feature at around 536eV consistent with the feature observed in O K-edge XAS spectrum of Na-O_2 electrolyte (Fig.S1, Supporting Information) and previously reported discharge products[12, 16]. This peak is associated with the transition of electron from O1s to σ^* antibonding states. With the deposition of discharge product during the discharge process, a peak gradually emerges at 532eV. This peak is the O1s to π^* transition of the O_2^- anions, indicating the nucleation and deposition of NaO_2 discharge product on the gold coated cathode. With progression of the discharge process, the intensity of the π^* transition peak raises, indicating the increase in deposition and ordering of NaO_2 on the surface of the electrode respectively.

During the charge process, the behavior of the π^* transition peak is reversed. At the end of the charge cycle, the fingerprint feature of π^* transition disappears. However, there is a small broad feature remaining in the XAS spectra at around 532 to 534eV which can be correlated to the presence of decomposed NaO_2 or formation of side products at the electrode/electrolyte interface.

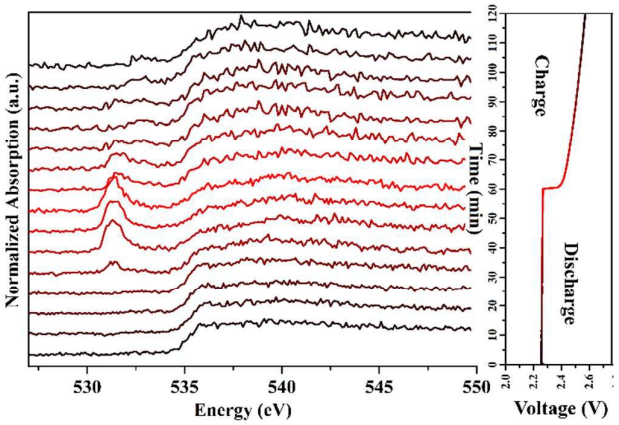

Figure 2. O K-edge XAS PFY spectra of cathode in the Na-O_2 cell. The data were collected in-situ with electrochemical cycling for two hours.

Scanning electron microscopy (SEM) of the cathode electrode after discharge process (Fig. S3a, Supporting Information) confirms the formation of discharge products on the surface of the cathode window. Unlike the typical cubic shaped micron-sized NaO_2 discharge products usually reported for carbon-based cathodes[2, 7], a conformal film of products was observed on the window along with irregular products on top of the films. The SEM images of fully charged gold coated window reveal the decomposition of majority of NaO_2 discharge product on the electrode surface (Fig. S3b, Supporting Information). However, small areas with thin film coatings of the discharge products remain which are likely responsible for the broad weak feature seen in fully charged O K-edge XAS spectra of the cathode electrode.

Formation of conformal products film on Au surface can be attributed to the surface mediated growth mechanism on Au cathode[24]. To confirm the effect of air electrode substrate on the morphology and nature of the products, we examined the morphology of discharge products in Na-O_2 cells using pristine and gold coated carbon cathodes. Unlike uncoated carbon electrode (Fig. S4a, b, Supporting Information) where cubic NaO_2 was observed, the discharge products form a thin film uniformly covering the surface of the gold-coated air electrode (Fig. S4c, d, Supporting Information). Similar results have also been reported in Li-O_2 cells, where changes in the cell behavior[25, 26] and discharge product morphology[27] were shown by application of noble metal.

View Article Online
DOI: 10.1039/C8EE00721G

Raman spectroscopy measurements (Fig. S5, Supporting Information) of the discharge products formed on gold coated cathodes (on both gold coated silicon nitride windows and gold coated carbon electrodes), confirm the formation of NaO_2 on the cathode immediately after discharge, as indicated in previous work[2].

There has been a debate over the stability of discharge products in Na-O_2 batteries.[7, 10, 14, 15, 28] On one side, NaO_2 is argued to reversibly form and decompose during the discharge and charge cycles of Na-O_2 cells without any side reactions.[2, 7, 29] On the other side, it has been shown that NaO_2 discharge products may gradually transform into $Na_2O_2.H_2O$ or Na_2CO_3 side-products as a result of decomposition reaction of cell electrolyte and/or air electrode.[10, 14-16, 30] Formation of side-products in Na-O_2 cells results in significantly increased charging over-potential as well as decreased Coulombic efficiency. We have used the micron level mapping capability of the in-situ XAS technique to track the chemical changes occurring in the discharge products formed in Na-O_2 cells in contact with the cell electrolyte.

To study the stability of discharge products, a discharged Na-O_2 cell was set to rest in an open circuit voltage for 3 hours. The discharge product exhibited the fingerprint feature of NaO2 at 532eV after 3 hours of rest in the cell environment (Fig. S6, Supporting Information). However, non-symmetrical broadness of the peak and the shoulder peak appearing at around 533.5eV, can be associated with slight changes in the local environment of O_2^{-2} or formation other more stable compounds. A broad feature (between 532 to 534eV) was observed on the cathode during the charge process (Fig. 2), indicating the formation of side products during discharge/charge process. A similar feature was observed by Medarno et al.[31], using transmission X-ray microscopy, which has been correlated to the presence of O deficient layer and shell of secondary products surrounding the NaO_2 discharge products. O K-edge spectra measured in a line-scan across the cathode window (Fig.S7, Supporting Information) illustrate changes between the ratio of peak featured at 532eV and new peak centered around 533.5eV across the cathode. Based on changes observed in the O K-edge XAS spectrum (Fig. S7, Supporting Information), we collected the fluorescence intensity of the oxygen emission lines ($K\alpha_2$) at several excitation energies (532eV, 533.5eV and 600eV) over the surface of the cathode window. This resulted in 2-dimentional maps of the distribution of discharge products and side products across the cathode electrode with a spatial resolution of around 20µm × 20µm. The processed maps were plotted for signals collected at 532eV (Fig. 3a) and 533.5eV (Fig. 3b). Accordingly, the map obtained at 532eV represents NaO_2 products, while the map at 533.5eV is associated with the side-products formed during the rest period.

At 532eV, there is a gradient in the concentration of oxygen fluorescence intensity across the Si_3N_4 window (Fig. 3a). This is in good agreement with previous results, confirming the formation of thin film discharge products (NaO_2) over gold coated electrodes (Fig. S3a, Supporting Information). The gradient in the concentration of oxygen is as a result of detector vs window positioning. However, at 533.5eV, the map of fluorescence intensity of oxygen emission line shows several islands of high concentration and non-uniform distribution of products on the Si_3N_4 windows (Fig. 3b). This represents the non-uniform formation of side products on gold coated Si_3N_4 windows. Similar results were observed on data collected using detectors position at ~0^o angle with respect to the cathode window (Fig. S8a, b, Supporting Information).

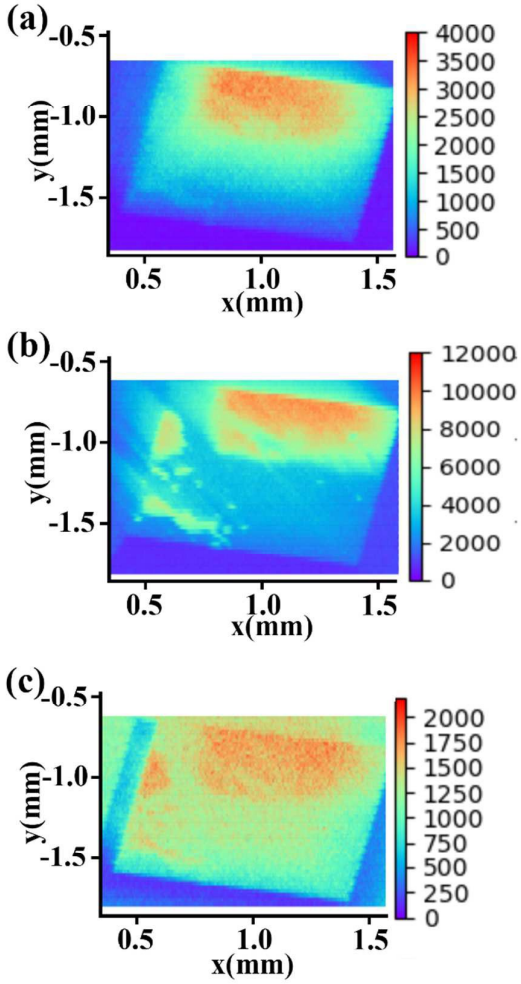

Figure 3. Oxygen emission line ($K\alpha_2$) XRF maps of the cathode window collected using 450 angle detectors at incident energy of (a) 532eV [NaO_2 product], (b) 533.5 eV [side products]. (c) XRF map based on carbon emission line ($K\alpha_2$) of the cathode window at incident energy of 533.5eV.

The 2-dimentional map, generated from fluorescence intensity of carbon emission line ($K\alpha_2$) collected at the above excitation energies from the Si_3N_4 window, can further clarify the nature of these discharge products. The carbon-based fluorescence intensity maps generated from detectors at angles close to 0^0 (shallow probing depth), show a negligible concentration of carbon, uniformly distributed across the Si_3N_4 window (Fig. S8c, Supporting Information). Maps plotted based on data

View Article Online
DOI: 10.1039/C8EE00721G

collected by detectors positioned at 45° to the window (deeper probing depth), present a non-uniform distribution of carbon on the window, closely following the distribution of oxygen maps obtained at 533.5eV (Fig. 3c). These results confirm the formation of NaO_2 as the main discharge product as films on the surface of the cathode (gold coated Si_3N_4 window). Furthermore, during the rest period, as illustrated in the figure 3, side products containing carbon, oxygen and sodium are formed and non-uniformly distributed on the interface of NaO_2 discharge product and electrolyte. These results are in accordance with the previously reports on the formation of $Na_2O_2.2H_2O$, sodium acetate or sodium formate at the NaO_2/electrolyte interface.[10, 14, 32]

The charging response of the discharge products of Na-O_2 cells was examined before and after 3 hours rest period to evaluate the effect of side-products on the charging characteristics of the cell. The results (Fig. S9, Supporting Information) indicate after 3 hours of rest, in addition to loss of capacity, the Na-O_2 cell exhibits an initial spike of potential during the charge cycle. A similar spike in charging behavior has been previously reported for Na-O_2 cells.[12, 14] Such an increase in charging overpotential is limited to a very short period before the potential is lowered to charge potential consistent with the decomposition of NaO_2. This initial increase of charging overpotential has been correlated to the dissolution of NaO_2 into the cell electrolyte[33]. However, our in-situ analysis illustrates that the formation of side-products at the interface of NaO_2 discharge product with the cell electrolyte can be an additional factor for the initial increase of charging overpotential. A thin film surrounding the surface of NaO_2 discharge products formed during the rest period acts as an initial barrier during the charge process. After an initial spike in the voltage to overcome this barrier, the charge potential decreases to the values associated with NaO2 decomposition.[2, 14, 16]

Conclusions

In summary, we developed an in-situ soft XAS technique to track the formation and decomposition of discharge products in a working Na-O_2 cell by monitoring the O K-edge XAS spectrum at the positive electrode of the cell. The results indicated reversible formation and decomposition of irregular structures and conformal film-like NaO_2 on the surface of Au air electrode during the discharge/charge cycles, respectively. We also examined the stability of NaO_2 discharge products in the Na-O_2 cell environment by XAS mapping of the changes in the composition of deposited NaO_2. The results illustrated that a non-uniform layer of side-products formed on the surface of NaO_2, likely as a result of decomposition reaction between the discharge product and the cell electrolyte. Further studies are needed to determine the nature of this phase and its implication in charge and discharge processes of Na-O_2 cells. The present study illustrates the capability of in-situ soft XAS technique in illuminating the underlaying mechanisms of charge/discharge processes in metal-O_2 batteries. It is expected that the developed in-situ soft XAS cell can be further modified for other types of metal-O_2 batteries, metal-ion batteries and fuel cells studies.

Conflicts of interest

There are no conflicts to declare.

Acknowledgements

This research was supported by National Science and Engineering Research Council of Canada, Canada Research Chair, and the Interdisciplinary Initiative (IDI) of Western University. The research described in the paper was performed at the Canadian Light Source which is supported by CFI, NSERC, CHIR, NRC, and the University of Saskatchewan.

References

1. W.-W. Yin and Z.-W. Fu, *ChemCatChem*, 2017, 9, 1545-1553.
2. P. Hartmann, C. L. Bender, M. Vracar, A. K. Durr, A. Garsuch, J. Janek and P. Adelhelm, *Nat Mater*, 2013, **12**, 228-232.
3. H. Yadegari, Q. Sun and X. L. Sun, *Adv Mater*, 2016, **28**, 7065-7093.
4. B. Chen, H. Lu, J. Zhou, C. Ye, C. Shi, N. Zhao and S. Z. Qiao, *Adv Energy Mater*, 2018, , 1702909.
5. F. X. Xie, L. Zhang, D. W. Su, M. Jaroniec and S. Z. Qiao, *Adv Mater*, 2017, **29**, 1700989.
6. N. Zhao and X. Guo, *J Phys Chem C*, 2015, **119**, 25319-25326.
7. C. Xia, R. Black, R. Fernandes, B. Adams and L. F. Nazar, *Nat Chem*, 2015, **7**, 496-501.
8. C. Xia, R. Fernandes, F. H. Cho, N. Sudhakar, B. Buonacorsi, S. Walker, M. Xu, J. Baugh and L. F. Nazar, *J Am Chem Soc*, 2016, **138**, 11219-11226.
9. P. Hartmann, M. Heinemann, C. L. Bender, K. Graf, R.-P. Baumann, P. Adelhelm, C. Heiliger and J. Janek, *J Phys Chem C*, 2015, **119**, 22778-22786.
10. J. Kim, H. Park, B. Lee, W. M. Seong, H. D. Lim, Y. Bae, H. Kim, W. K. Kim, K. H. Ryu and K. Kang, *Nat Commun*, 2016, **7**, 10670.
11. D. Schröder, C. L. Bender, R. Pinedo, W. Bartuli, M. G. Schwab, Ž. Tomović and J. Jürgen, *Energy Technol*, 2017, **5**, 1242-1249.
12. R. Morasch, D. G. Kwabi, M. Tulodziecki, M. Risch, S. Zhang and Y. Shao-Horn, *ACS Appl Mater Interfaces*, 2016, **9**, 4374-4381.
13. R. Pinedo, D. A. Weber, B. Bergner, D. Schröder, P. Adelhelm and J. Janek, *J Phys Chem C*, 2016, **120**, 8472-8481.
14. I. Landa-Medrano, R. Pinedo, X. Bi, I. Ruiz de Larramendi, L. Lezama, J. Janek, K. Amine, J. Lu and T. Rojo, *ACS Appl Mater Interfaces*, 2016, **8**, 20120-20127.
15. S. Y. Sayed, K. P. Yao, D. G. Kwabi, T. P. Batcho, C. V. Amanchukwu, S. Feng, C. V. Thompson and Y. Shao-Horn, *Chem Commun (Camb)*, 2016, **52**, 9691-9694.
16. H. Yadegari, M. N. Banis, B. W. Xiao, Q. Sun, X. Li, A. Lushington, B. Q. Wang, R. Y. Li, T. K. Sham, X. Y. Cui and X. L. Sun, *Chem Mater*, 2015, **27**, 3040-3047.
17. W. J. Kwak, Z. H. Chen, C. S. Yoon, J. K. Lee, K. Amine and Y. K. Sun, *Nano Energy*, 2015, **12**, 123-130.
18. Z. L. Jian, Y. Chen, F. J. Li, T. Zhang, C. Liu and H. S. Zhou, *J Power Sources*, 2014, **251**, 466-469.

View Article Online
DOI: 10.1039/C8EE00721G

19. Q. Sun, H. Yadegari, M. N. Banis, J. Liu, B. W. Xiao, X. Li, C. Langford, R. Y. Li and X. L. Sun, *J Phys Chem C*, 2015, **119**, 13433-13441.
20. Q. Sun, H. Yadegari, M. N. Banis, J. Liu, B. W. Xiao, B. Q. Wang, S. Lawes, X. Li, R. Y. Li and X. L. Sun, *Nano Energy*, 2015, **12**, 698-708.
21. T. Regier, J. Krochak, T. K. Sham, Y. F. Hu, J. Thompson and R. I. R. Blyth, *Nucl Instrum Meth A*, 2007, **582**, 93-95.
22. S. Yang and D. J. Siegel, *Chem Mater*, 2015, **27**, 3852-3860.
23. J. S. Kang, D. H. Kim, J. H. Hwang, J. Baik, H. J. Shin, M. Kim, Y. H. Jeong and B. I. Min, *Physical Review B*, 2010, **82**, 193102.
24. N. B. Aetukuri, B. D. McCloskey, J. M. Garcia, L. E. Krupp, V. Viswanathan and A. C. Luntz, *Nat Chem*, 2015, **7**, 50-56.
25. Z. Q. Peng, S. A. Freunberger, Y. H. Chen and P. G. Bruce, *Science*, 2012, **337**, 563-566.
26. M. M. O. Thotiyl, S. A. Freunberger, Z. Q. Peng, Y. H. Chen, Z. Liu and P. G. Bruce, *Nat Mater*, 2013, **12**, 1049-1055.
27. X. Y. Luo, M. Piernavieja-Hermida, J. Lu, T. P. Wu, J. G. Wen, Y. Ren, D. Miller, Z. Z. Fang, Y. Lei and K. Amine, *Nanotechnol*, 2015, **26**, 164003.
28. C. L. Bender, P. Hartmann, M. Vračar, P. Adelhelm and J. Janek, *Adv Energy Mater*, 2014, **4**, 1301863.
29. B. D. McCloskey, J. M. Garcia and A. C. Luntz, *J Phys Chem Lett*, 2014, **5**, 1230-1235.
30. Y. C. Lu and Y. Shao-Horn, *J Phys Chem Lett*, 2013, **4**, 93-99.
31. I. Landa-Medrano, A. Sorrentino, L. Stievano, I. Ruiz de Larramendi, E. Pereiro, L. Lezama, T. Rojo and D. Tonti, *Nano Energy*, 2017, **37**, 224-231.
32. R. Black, A. Shyamsunder, P. Adeli, D. Kundu, G. K. Murphy and L. F. Nazar, *Chemsuschem*, 2016, **9**, 1795-1803.
33. B. D. McCloskey, D. S. Bethune, R. M. Shelby, G. Girishkumar and A. C. Luntz, *J Phys Chem Lett*, 2011, **2**, 1161-1166.